
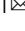





Record winter winds in 2020/21 drove exceptional Arctic sea ice transport

R. D. C. Mallett¹  , J. C. Stroeve^{1,2,3}, S. B. Cornish⁴ , A. D. Crawford³ , J. V. Lukovich³, M. C. Serreze², A. P. Barrett², W. N. Meier², H. D. B. S. Heorton¹  & M. Tsamados¹

The volume of Arctic sea ice is in decline but exhibits high interannual variability, which is driven primarily by atmospheric circulation. Through analysis of satellite-derived ice products and atmospheric reanalysis data, we show that winter 2020/21 was characterised by anomalously high sea-level pressure over the central Arctic Ocean, which resulted in unprecedented anticyclonic winds over the sea ice. This atmospheric circulation pattern drove older sea ice from the central Arctic Ocean into the lower-latitude Beaufort Sea, where it is more vulnerable to melting in the coming warm season. We suggest that this unusual atmospheric circulation may potentially lead to unusually high summer losses of the Arctic's remaining store of old ice.

¹Centre for Polar Observation and Modelling, Earth Sciences, University College London, London, UK. ²National Snow and Ice Data Center, CIRES, University of Colorado, Boulder, CO, USA. ³Centre for Earth Observation Science, University of Manitoba, Winnipeg, Canada. ⁴Department of Earth Sciences, University of Oxford, Oxford, UK. ✉email: robbie.mallett.17@ucl.ac.uk

The age, extent, thickness and volume of Arctic sea ice are in multidecadal decline^{1,2}. However, these quantities all exhibit year-to-year variability, which is in part determined by variable atmospheric circulation patterns (e.g. Stroeve et al.³). The average large-scale winter Arctic sea ice circulation comprises the anticyclonic (clockwise) Beaufort Gyre^{4,5}, cyclonic circulation in the Eurasian shelf seas, and the linear Transpolar Drift Stream between these two regions⁶. The strength and separability of these features are controlled by the position and strength of the Beaufort Sea High (BSH)⁷ typically centred over the Canada Basin, and a trough of low sea-level pressure (SLP) extending into the Barents and Kara Seas associated with the northern terminus of the North Atlantic cyclone track. A strong BSH is associated with strong anticyclonic winds, resulting in a strong Beaufort Gyre⁸. This acts to recirculate older, thicker ice around the Arctic Ocean. BSH strength and position is in part related to the Arctic Oscillation (AO)⁹, the leading mode of Northern Hemisphere SLP variability north of the Tropics¹⁰. The AO is an annular mode centred roughly over the pole and linked to the stratospheric polar vortex.

The winter of 2020/21 was highly unusual, featuring an extremely strong BSH and accompanying anticyclonic winds in the central Arctic. The December–January–February (DJF) period had the second highest mean SLP north of 60°N since 1979 (Fig. 1a, b), associated with the second most negative (anticyclonic) index value of the AO in the same period (Fig. 1c, d), only surpassed by the winter of 2009/2010. These conditions occurred in the context of a sudden stratospheric warming event that began on January 5, 2021 (Fig. 1g). The extreme anticyclonic winds strengthened and broadened the Beaufort Gyre circulation, enhancing the transport of sea ice both into and out of the Beaufort Sea. This transport flushed first-year ice from the region and resulted in the Beaufort Sea containing the largest fraction (23.5%) of the Arctic's multiyear ice area at winter's end since the record began in 1984. This multiyear ice will be highly vulnerable to melting out in summer 2021 in the warm waters of this region, further reducing the Arctic store of multiyear ice and hastening the transition to a seasonally ice-free Arctic Ocean.

To set the stage, we first characterise the atmospheric circulation in winter (DJF) from 1979/1980 to 2020/2021 using data from the ERA5 atmospheric reanalysis¹¹. We calculate the mean SLP north of 60°N and the vorticity of the 10-m winds over the Arctic Ocean sea ice (defined using monthly ice concentration data¹²). We also (where possible) determine the mean position of the BSH from the location of the DJF SLP maximum. We contextualise this analysis with a daily and seasonally averaged AO index.

We next explore the impact of the exceptional BSH in the winter of 2020/2021 on the sea ice cover. We first analyse weekly ice area flux through gates following Stroeve et al.³ for the winters of 1979–2021. We also determine the area-fraction of Arctic multiyear ice transported through the gates and that ultimately resided in the Beaufort Sea at the end of winter. Finally, we investigate the volume-fraction of total Arctic Ocean sea ice that resided in a “Survival Zone” at the end of February. We define this zone as the area where sea ice is present on the 1st of September in more than 50% of years over the last decade (Fig. 2h).

Results

As seen in Fig. 1, a record high in SLP poleward of 60°N occurs on 11th February, following a sudden stratospheric warming event on January 5, 2021 (Fig. 1g). This contributed to the second-highest winter SLP since 1979, as well as the second-most negative AO index in the same period (Fig. 1b, d), only surpassed in winter 2009/2010. We note that sudden stratospheric warming was also present and characterised the winter atmospheric and sea ice circulation in 2018¹³.

A measure of anticyclonic flow is the relative vorticity⁷. Relative vorticity of the 10-m winds over Arctic Ocean sea ice fell more than 2.3 standard deviations below 1979–2021 mean (Fig. 1f; $-0.96 \times 10^{-5} \text{ s}^{-1}$). While the AO index during winter 2020/2021 was not at a record negative value, the positioning of the BSH was partially responsible for this record low value. Because the BSH is a semi-permanent feature⁴, we are able to identify its DJF-mean position for 18 years of our 42-year record including 2020/2021 (Figs. S1–S3). During winter 2020/2021 the BSH was positioned further northward and further westward than any previous year (Fig. 1h). The BSH persisted such that the corresponding winter SLP anomaly had a highly prominent maximum value (compared to other local maxima in the Arctic) by comparison to previous years. The poleward shift of the BSH centre allowed the anomalously high pressure to translate into a record anticyclonic wind forcing of the sea ice. We justify this statement by pointing out that there is a statistically significant and negative correlation ($p = 0.6\%$; $r = -0.62$) between the latitude of the BSH and the wind-vorticity over sea ice in the eighteen years where we identified BSH position (Fig. S4).

We now characterise the sea ice response to the exceptional wind forcing. The sea ice area flux from the Beaufort Sea into the Chukchi Sea was the largest since 1979, and flux from the central Arctic Ocean into the Beaufort Sea is the second largest (exceeded by winter 2012/2013) (Fig. 2a, b). We show that these anomalous fluxes result directly from the record-anticyclonic wind forcing by regressing the DJF wind vorticity over Arctic Ocean sea ice against the winter areal ice fluxes; there is a strong linear relationship between the two variables for both gates ($r \geq 0.78$) (Fig. 2c, d). This regression is considerably more robust than that of ice fluxes against the DJF AO index (Fig. S5). A back-tracking analysis using the ice motion vectors shows that ice crossing the flux gate in the last full week of February had travelled approximately perpendicularly to the gate over the previous 12 weeks, and in the first full week of December lay between 300 and 400 km away from the gate, north of the Canadian Archipelago (Fig. S6). This places it roughly within the western “last ice area” as defined by Moore et al.¹⁴—winter ice fluxes into and out of this region are particularly relevant to the persistence of sea ice in summer over the next century.

We now consider the ramifications of this anomalous sea ice motion on the evolution of the sea ice cover, with particular reference to the Arctic's shrinking cover of old (multiyear; MYI) ice. We first note that there are some differences between the direction of the wind-forcing of the ice and the ice motion itself due to Ekman dynamics and rheology¹⁵: these broadly had the effect of deflecting the sea ice on average by around 20° to the right in the Western Arctic Ocean in DJF 2021, with the ice moving on average at 1–3% of the average wind speed (Fig. S7, S8). The response of the sea ice to the wind forcing was such that four times as much MYI area was transported into the Beaufort Sea as was transported out, but the total ice area transported out was double that transported in (Fig. 2a, b). This transport acted to flush the Beaufort Sea of its first-year ice cover and fill it with MYI. Eight per cent of the Arctic's MYI cover was transported into the Beaufort Sea in winter 2020/2021 (Fig. 2e), contributing to a record fraction of the MYI cover residing in the Beaufort Sea (23.5%) in the last full week of February (Fig. 2f). This fraction has been historically increasing over the data period (1983–2020), however, this high concentration is well above the linear trend (by 2.06 standard deviations; Figs. S9 and S10). Because around two-thirds of the Beaufort Sea has been ice-free on the first of September over the last decade (Fig. 2h), this unprecedented concentration of Arctic MYI in the Beaufort Sea puts it at a larger risk of melting.

Measurements from CryoSat-2 indicate that the volumetric fraction of Arctic Ocean sea ice residing in the Chukchi Sea at the end of winter has also been in a statistically significant decline over the last decade (Fig. S11; 2.3% per decade, $p = 0.0045$). The unusual

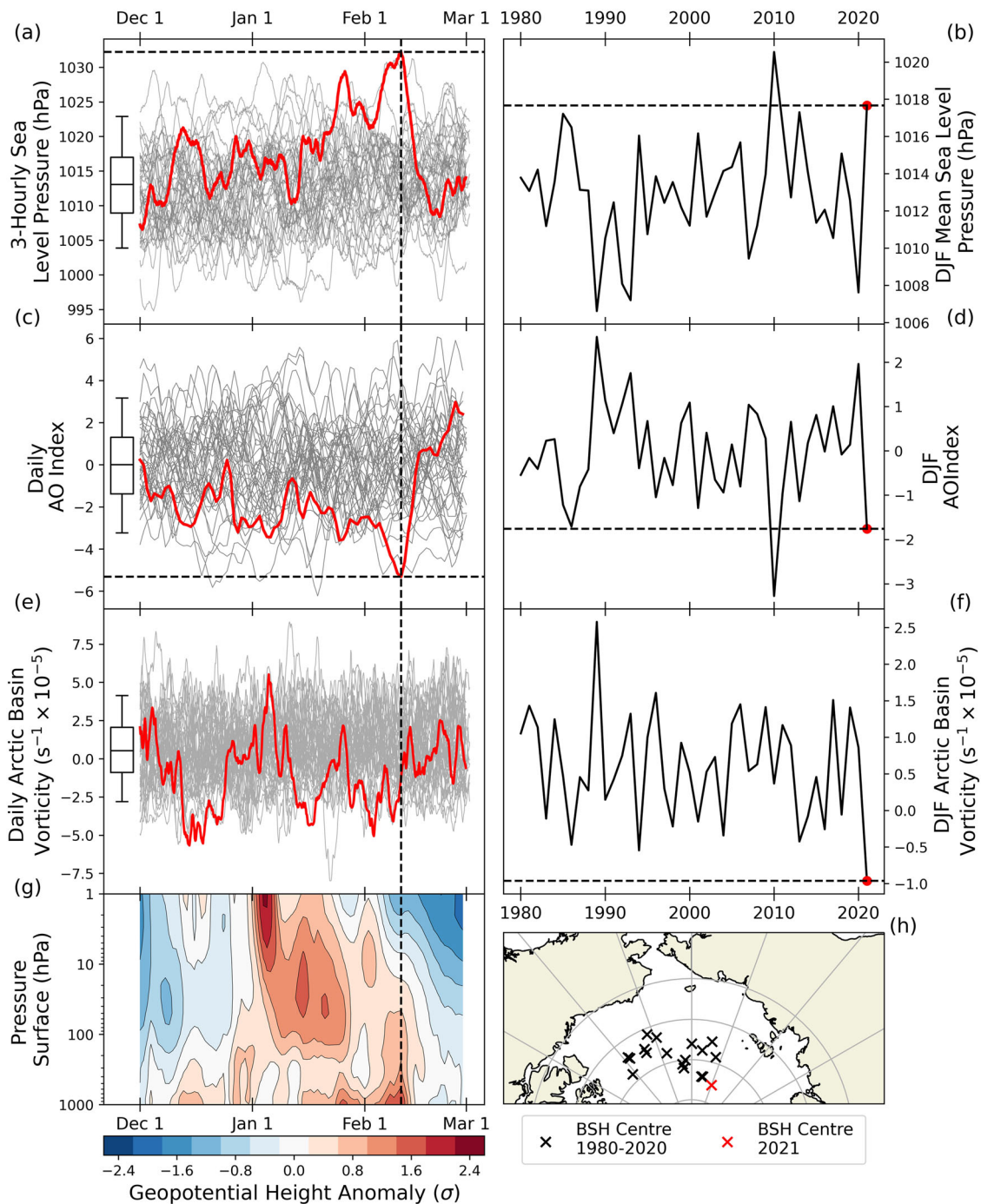


Fig. 1 Atmospheric conditions in winter 2020/2021. **a** Three-hourly SLP north of 60°N for all winters 1979–2021 with winter 2020/21 in red. **b** DJF SLP averaged over the same period and area. **c** Daily Arctic Oscillation index from NOAA in the same period with 2020/2021 in red. **d** DJF AO index for DJF in the same period. **e** Three-hourly vorticity of 10-m winds over Arctic Ocean sea ice. Box-and-whisker plots in panels **(a, c, e)** represent the median and interquartile and 5/95% DJF ranges of the plotted quantities. **f** DJF integrated vorticity over sea ice. **g** Geopotential height anomalies for the DJF 2020/21 period showing a sudden stratospheric warming event on January 5, 2021. **h** The position of the Beaufort Sea High centre for 18 years where it could be resolved against other high pressure systems.

atmospheric circulation in the winter of 2020/2021 contributed to a departure from this trend. At the end of February, the Chukchi sea held an above-mean and above-median fraction of the Arctic Ocean sea ice (Fig. S11). When the winter of 2020/2021 is considered, the decline is slower and less statistically significant (1.6% per decade, $p = 0.037$). Sea ice in the Chukchi Sea is highly vulnerable to summer melting due to general warming of the upper ocean, influenced in part by a warming Pacific inflow through Bering Strait^{16,17}.

Finally, the total end-of-winter 2020/2021 volume of ice in the “survival zone” was at a record low since the CryoSat-2 time-series began in winter 2010/2011, marginally beating 2013 (Fig. 2g). We do, however, note that radar-altimetry derived estimates of sea ice thickness and volume are subject to large uncertainties involving waveform interpretation¹⁸ and snow cover¹⁹. The shape of this survival zone (Fig. 2h) is closely aligned with contours of mean surface and 925 hPa air temperature (Fig. S12). The transport of MYI

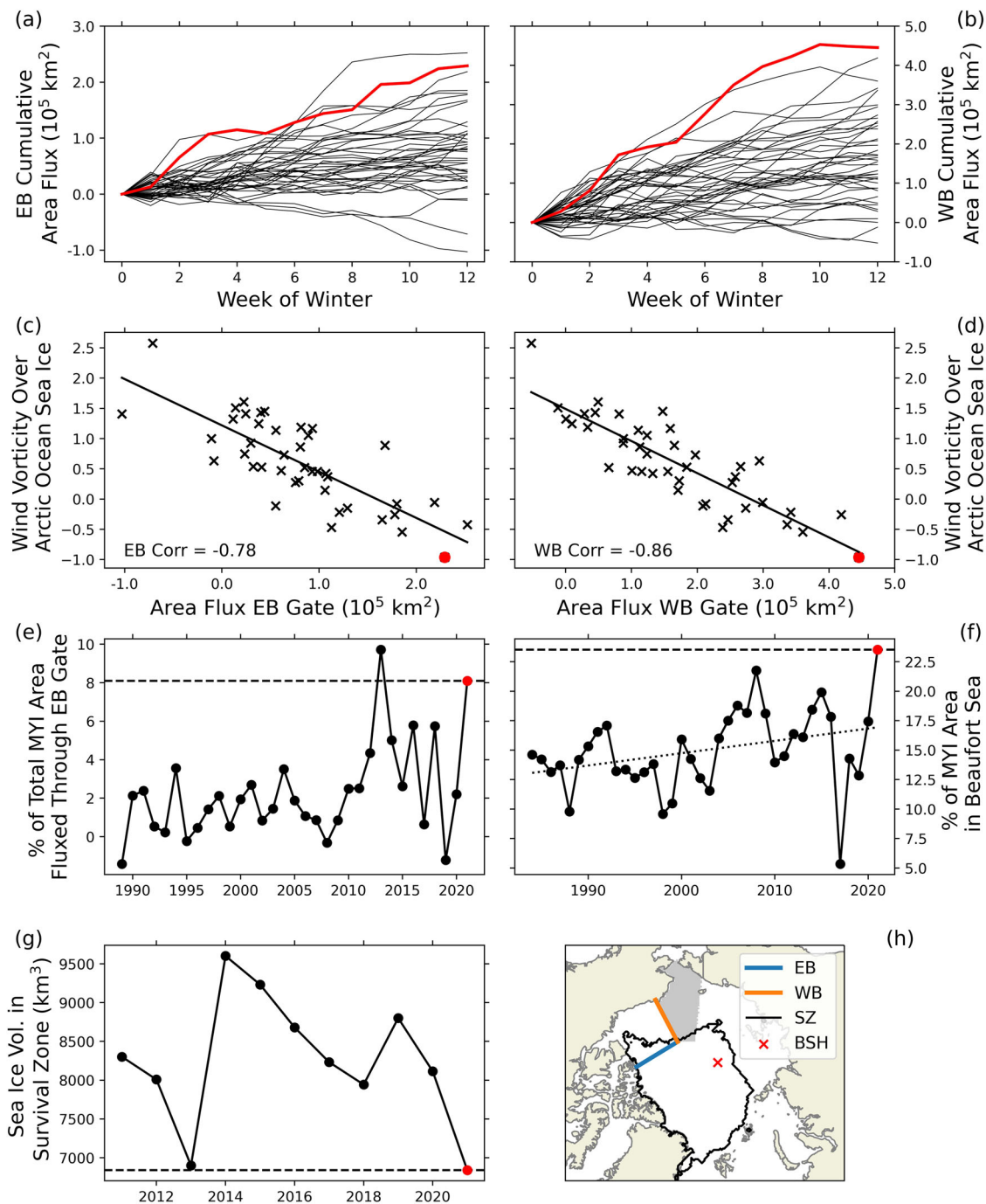


Fig. 2 Sea ice response to anomalous wind-forcing in winter 2020/2021. **a** Sea ice area flux from the central Arctic to the Beaufort Sea via the East Beaufort (EB) gate. **b** Flux from the Beaufort Sea to the Chukchi Sea via the West Beaufort (WB) gate. **c** Linear regression between the 10-m wind-vorticity over sea ice and areal flux through the EB gate. **d** Same as **c** but for the WB gate. **e** Percentage of Arctic multiyear ice area transported into the Beaufort Sea via the East Beaufort gate in the 12-week winter period. **f** Percent of Arctic MYI area within the Beaufort Sea in last full week of February. **g** Volume of Arctic Ocean sea ice in “survival zone” on Feb 28. **h** The position of the two flux gates used in this paper, the region of the Chukchi Sea (grey shading), and the position of the 2020/2021 BSH (red cross, as in Fig. 1h). The Beaufort Sea is enclosed by the two Beaufort gates. The black contour line indicates the “survival zone”.

out of this climatologically colder, the safer zone may well precipitate a record low in MYI coverage and sea ice volume. At the same time, record low sea ice thickness within the survival zone could lead to increased vulnerability of the sea ice within the zone²⁰.

In conclusion, we show that unusually high SLP over the central Arctic Ocean in the winter of 2020/2021 led to the strongest anticyclonic wind forcing on the sea ice since 1979. This forcing was directly responsible for record ice-area-flux from the Beaufort Sea into the Chukchi Sea. It also contributed to a record

fraction of the Arctic’s older ice being sequestered in the Beaufort Sea. This anomalous redistribution of ice to regions that are typically ice-free at the summer minimum may foreshadow large losses of the Arctic’s old ice over the summer.

Methods

We produced a DJF time-series for sea ice age using the weekly ice age product of the NSIDC which extends from 1984 to 2019 inclusive²¹. We defined multiyear ice as all ice where the sea ice age was 2-years or above. We used the Quicklook²² product for ice

ages in 2020 and 2021. We defined the DJF period as a 12-week time period that began in the first full week of December and ended in the last full week of the following February. An identical process was used to produce a DJF series of ice area fluxes back to 1979 using the NSIDC weekly ice motion products^{23,24}. To calculate sea ice fluxes it was necessary to weight the grid cells by the ice concentration. Concentration data was also required to define the ice-covered area for calculation of mean wind vorticity over sea ice and for the definition of the “survival zone”. This was done using data from Meier et al.¹². Technical details for reproducing our flux calculations are given in the supplement (Section S1).

For calculations of sea ice volume distribution, we used the merged CryoSat-2/SMOS dataset from Ricker et al.²⁵. This has a weekly time resolution and is released on a daily timestep. Our volume calculations characterised the last day of February so we selected the week of data centred on this day.

Data for 10 m winds, 2 m and 925 hPa temperatures, and SLP was taken from the ERA5 atmospheric reanalysis¹¹. We produced a three-hourly time series that extended from 00:00 UTC at the beginning of December to 21:00 on the last day of the following February, respectively, from 1979 to 2021.

Data availability

All data used in this study are publicly available on the internet for download. The Arctic Oscillation index was downloaded from NOAA (https://www.cpc.ncep.noaa.gov/products/precip/CWlink/daily_ao_index/ao_index.html, Accessed on 2 April 2021). The ERA5 atmospheric reanalysis data¹¹ were downloaded from the Copernicus Climate Change Service Climate Data Store (<https://cds.climate.copernicus.eu/cdsapp#!/home>). The sea ice concentration, sea ice motion, sea ice age, products were downloaded from the NSIDC website, with respective URLs available in the references section^{12,21–24}. The sea ice thickness data²⁵ were downloaded from the Alfred Wegener Institute website (<https://spaces.awi.de/display/CS2SMOS/CryoSat-SMOS+Merged+Sea+Ice+Thickness>).

Code availability

All code required to reproduce the analysis can be found at <https://www.github.com/robbiemallett/BSH>

Received: 23 April 2021; Accepted: 7 July 2021;

Published online: 03 August 2021

References

- Stroeve, J. & Notz, D. Changing state of Arctic sea ice across all seasons. *Environ. Res. Lett.* **13**, 103001 (2018).
- Kwok, R. Arctic sea ice thickness, volume, and multiyear ice coverage: Losses and coupled variability (1958–2018). *Environ. Res. Lett.* **13**, 105005 (2018).
- Stroeve, J. et al. Sea ice response to an extreme negative phase of the Arctic Oscillation during winter 2009/2010. *Geophys. Res. Lett.* <https://doi.org/10.1029/2010GL045662> (2011).
- Armitage, T. W., Manucharyan, G. E., Petty, A. A., Kwok, R. & Thompson, A. F. Enhanced eddy activity in the Beaufort Gyre in response to sea ice loss. *Nat. Commun.* **11**, 1–8 (2020).
- Petty, A. A., Hutchings, J. K., Richter-Menge, J. A. & Tschudi, M. A. Sea ice circulation around the Beaufort Gyre: the changing role of wind forcing and the sea ice state. *J. Geophys. Res.* **121**, 3278–3296 (2016).
- Kwok, R., Spreen, G. & Pang, S. Arctic sea ice circulation and drift speed: decadal trends and ocean currents. *J. Geophys. Res.* **118**, 2408–2425 (2013).
- Serreze, M. C. & Barrett, A. P. Characteristics of the Beaufort Sea high. *J. Clim.* **24**, 159–182 (2011).
- Regan, H. C., Lique, C. & Armitage, T. W. K. The Beaufort Gyre extent, shape, and location between 2003 and 2014 from satellite observations. *J. Geophys. Res.* **124**, 844–862 (2019).
- Rigor, I. G., Wallace, J. M. & Colony, R. L. Response of sea ice to the Arctic Oscillation. *J. Clim.* **15**, 2648–2663 (2002).
- Thompson, D. W. J. & Wallace, J. M. The Arctic oscillation signature in the wintertime geopotential height and temperature fields. *Geophys. Res. Lett.* **25**, 1297–1300 (1998).
- Hersbach, H. et al. ERA5 monthly averaged data on pressure levels from 1979 to present. (Copernicus Climate Change Service (C3S) Climate Data Store (CDS), accessed 2 April 2020) (2019).
- Meier, W. et al. NOAA/NSIDC Climate Data Record of Passive Microwave Sea Ice Concentration, Version 3. (NSIDC: National Snow and Ice Data Center. Boulder, Colorado USA, accessed 2 April 2021). <https://nsidc.org/data/g02202> (2017).
- Moore, G. W., Schweiger, A., Zhang, J. & Steele, M. What caused the remarkable february 2018 North Greenland Polynya? *Geophys. Res. Lett.* **45**, 342–13 (2018).
- Moore, G. W., Schweiger, A., Zhang, J. & Steele, M. Spatiotemporal variability of sea ice in the Arctic's last ice area. *Geophys. Res. Lett.* **46**, 11237–11243 (2019).
- Heorton, H. D. et al. Retrieving Sea Ice Drag coefficients and turning angles from in situ and satellite observations using an inverse modeling framework. *J. Geophys. Res.* **124**, 6388–6413 (2019).
- Woodgate, R. A., Weingartner, T. & Lindsay, R. The 2007 Bering Strait oceanic heat flux and anomalous Arctic sea-ice retreat. *Geophys. Res. Lett.* <https://doi.org/10.1029/2009GL041621> (2010).
- Serreze, M. C., Crawford, A. D., Stroeve, J. C., Barrett, A. P. & Woodgate, R. A. Variability, trends, and predictability of seasonal sea ice retreat and advance in the Chukchi Sea. *J. Geophys. Res.* **121**, 7308–7325 (2016).
- Ricker, R., Hendricks, S., Helm, V., Skourup, H. & Davidson, M. Sensitivity of CryoSat-2 Arctic sea-ice freeboard and thickness on radar-waveform interpretation. *Cryosphere* **8**, 1607–1622 (2014).
- Mallett, R. D. C. et al. Faster decline and higher variability in the sea ice thickness of the marginal Arctic seas when accounting for dynamic snow cover. *The Cryosphere* **15**, 2429–2450 (2021).
- Holland, M. M. & Stroeve, J. Changing seasonal sea ice predictor relationships in a changing Arctic climate. *Geophys. Res. Lett.* <https://doi.org/10.1029/2011GL049303> (2011).
- Tschudi, M., Meier, W., Stewart, J., Fowler, C. & Maslanik, J. EASE-Grid Sea Ice Age, Version 4. (NASA National Snow and Ice Data Center Distributed Active Archive Center, Boulder, Colorado USA, accessed 2 April 2021). <https://nsidc.org/data/nsidc-0611/versions/4> (2019).
- Tschudi, M., Meier, W. & Stewart, J. Quicklook Arctic Weekly EASE-Grid Sea Ice Age, Version 1. (NASA National Snow and Ice Data Center Distributed Active Archive Center, Boulder, Colorado USA, accessed 2 April 2021). <https://nsidc.org/data/nsidc-0749>.
- Tschudi, M., Meier, W., Stewart, J., Fowler, C. & Maslanik, J. Polar Pathfinder Daily 25 km EASE-Grid Sea Ice Motion Vectors, Version 4 (1979–2019). (NASA National Snow and Ice Data Center Distributed Active Archive Center, Boulder, Colorado USA, accessed 2 April 2021). <https://nsidc.org/data/nsidc-0116> (2019).
- Tschudi, M., Meier, W. & Stewart, J. Quicklook Arctic Weekly EASE-Grid Sea Ice Motion Vectors, Version 1. (NASA National Snow and Ice Data Center Distributed Active Archive Center, Boulder, Colorado USA, accessed 2 April 2021). <https://nsidc.org/data/nsidc-0748> (2019).
- Ricker, R. et al. A weekly Arctic sea-ice thickness data record from merged CryoSat-2 and SMOS satellite data. *Cryosphere* **11**, 1607–1623 (2017).

Acknowledgements

This work was funded primarily by the London Natural Environment Research Council (NERC) Doctoral Training Partnership (DTP) grant (NE/L002485/1). S.B.C.'s contribution was supported via a UK NERC DTP studentship (NE/L002612/1). J.C.S., J.L. and A.C. acknowledge support from the Canada 150 Chair Programme. J.C.S., W.N.M. and M.S. acknowledge support from the NASA-supported Arctic Sea Ice News and Analysis project (NNX16AJ92G). W.N.M.'s was also supported by the NASA Earth Science Data Information System (ESDIS) Project through the NASA Snow and Ice Distributed Active Archive Centre (DAAC) at NSIDC (80GSFC18C0102). M.T. acknowledges support from the European Space Agency “Polarice” grant ESA/AO/1-9132/17/NL/MP, NERC grant NE/S002510/1 and from the ESA “EXPRO + Snow” (ESA AO/1-10061/19/I-EF) project. MT and HH also acknowledge support from NERC “PRE-MELT” project (NE/T000546/1).

Author contributions

J.S. proposed the study and R.M. carried out the analysis. S.C., A.C., J.L., M.S., A.B., W.M., H.H. and M.T. contributed to the development of the study and writing of the paper.

Competing interests

The authors declare no competing interests.

Additional information

Supplementary information The online version contains supplementary material available at <https://doi.org/10.1038/s43247-021-00221-8>.

Correspondence and requests for materials should be addressed to R.D.C.M.

Peer review information *Communications Earth & Environment* thanks the anonymous reviewers for their contribution to the peer review of this work. Primary Handling Editors: Jan Lenaerts, Heike Langenberg.

Reprints and permission information is available at <http://www.nature.com/reprints>

Publisher's note Springer Nature remains neutral with regard to jurisdictional claims in published maps and institutional affiliations.



Open Access This article is licensed under a Creative Commons Attribution 4.0 International License, which permits use, sharing, adaptation, distribution and reproduction in any medium or format, as long as you give appropriate credit to the original author(s) and the source, provide a link to the Creative Commons license, and indicate if changes were made. The images or other third party material in this article are included in the article's Creative Commons license, unless indicated otherwise in a credit line to the material. If material is not included in the article's Creative Commons license and your intended use is not permitted by statutory regulation or exceeds the permitted use, you will need to obtain permission directly from the copyright holder. To view a copy of this license, visit <http://creativecommons.org/licenses/by/4.0/>.

© The Author(s) 2021